Peptide ^{17}O Chemical Shielding and Electric Field Gradient Tensors

Kevin W. Waddell,[†,‡] Eduard Y. Chekmenev,[§] and Richard J. Wittebort*[,†]

Department of Chemistry, 2320 South Brook Street, University of Louisville, Louisville, Kentucky 40292 and National High Magnetic Field Laboratory, Tallahassee, Florida 32310

Received: January 29, 2006; In Final Form: August 7, 2006

Complete ^{17}O chemical shielding (CS) and quadrupole coupling (QC) tensors and their molecular orientations were determined for the central residues in two tripeptides Gly-Gly-Val (GGV) and Ala-Gly-Gly (AGG) by single-crystal NMR methods. Tensor orientations in the two peptides are very similar, however, principal components are different. The most shielded CS and smallest magnitude QC components are normal to the peptide plane, while the most deshielded CS and largest QC components are in the peptide plane either at an angle of 17° (CS) or perpendicular (QC) to the C═O bond. Comparisons of principal components from experiment and DFT calculations indicate that the smaller shielding tensor span in GGV (549 ppm) compared to AGG (606 ppm) is likely due to two factors: a shorter "direct" H-bond distance to the peptide carbonyl oxygen and an "indirect" H bond of the peptide NH to a carboxylate rather than a carbonyl. We anticipate that ^{17}O NMR should be generally useful for probing H-bonding and local electrostatic interactions in proteins and polypeptides. Using the single-crystal data as an accurate reference, we show that a useful subset of the NMR parameters, QC and CS principal components and their relative orientation, can be obtained with reasonable accuracy from a very high-field (21.2 T), stationary sample powder spectrum.

Introduction

Carbonyl oxygen atoms occupy key locations in biomolecules. They stabilize biomolecular structure through hydrogen bonding and mediate dynamic processes such as catalysis and transport of water and ions. Compared to ^{1}H, ^{13}C, and ^{15}N, ^{17}O chemical shift (CS) dispersion is the largest (∼1500 ppm) of the NMR-active nuclei in protein backbones. In addition, the ^{17}O experiment reports directly on the electric field gradients from the surrounding electrons and charged groups by way of the quadrupole coupling (QC) interaction. Consequently, ^{17}O CS and QC parameters could complement structural information from these other nuclei in the study of biomolecules. However, solid-state ^{17}O NMR reports of biologically relevant compounds are sparse since the QC interaction complicates the NMR experiment in several ways. The number of parameters to be extracted from, for example, a powder spectrum is increased from three (CS principal components) to eight (CS and QC principal components and their relative orientation). In addition, quadrupolar broadening is a second-order effect and not completely averaged by the usual single-axis spinning (MAS) experiment. Finally, signal enhancement by cross-polarization in the MAS experiment is difficult because of a large, time-dependent first-order QC interaction during radio frequency excitation. Thus, well-resolved ^{17}O spectra with high S/N are difficult to collect.

Promising but technically demanding solutions to narrow quadrupolar broadening are dynamic-angle spinning (DAS),[1,2] double rotation (DOR),[3−5] and multiple quantum excitation with fast MAS (MQMAS).[6] High-resolution (∼1 ppm) ^{17}O spectra were recently reported for a series of amino acids using DOR[7] at modest (∼20%) levels of enrichment. Isotropic chemical shifts (δ_{iso}), quadrupolar coupling constants (χ), and the asymmetry parameters (η) were reported in this study, i.e., a subset of the 11 parameters that describe the full CS and QC tensors. Previously, Wu and co-workers[8] reported complete CS and QC tensors in non-peptide amides. They used DFT calculations to set initial estimates for extracting these parameters from powder data, and ultimately the absolute molecular orientations were inferred from the calculations. These workers noted the difficulties of correctly extracting the relevant parameters from the experimental data.[8] While superimposing dipolar couplings on spectra can be used to give a range of possible molecular orientations,[9,10] DOR, DAS, MAS, and static methods applied to unoriented samples provide subsets of ^{17}O CS and QC tensorial information with associated error limits that are inversely related to the total number of parameters extracted.

In this paper, we report single-crystal ^{17}O NMR studies of two crystallographically characterized tripeptides, AGG and GGV, labeled at the central peptide carbonyl. Tripeptides were selected because they readily crystallize, central residues capture essential features of protein amide linkages,[11,12] and analysis of the results by quantum chemical calculations of small clusters that include intermolecular interactions important in protein structure was possible. In combination with powder spectra, the single-crystal data unambiguously determined the complete set of NMR parameters: the CS and QC tensor principal components and their orientations in the molecular frame.[13] This complete characterization provides stringent tests of the quantum chemical analysis and is used to test the accuracy and uniqueness of a more facile method for extracting partial CS and QC tensor data from powder sample data. The methods described should be generally applicable since the peptides were prepared by solid-phase synthesis after the isotope was introduced directly into the Boc-glycine by exchange from $H_2{}^{17}O$ under basic conditions.

Considerable variations between GGV and AGG tensor principal components are observed, but molecular orientations of the principal axes are nearly identical in the two compounds.

* To whom correspondence should be addressed. E-mail: rjwitt01@louisville.edu.

† University of Louisville.

‡ Current address: Vanderbilt Institute of Imaging Science, Nashville, Tennessee 37212.

§ National High Magnetic Field Laboratory.

10.1021/jp060617o CCC: $33.50
Published on Web 10/19/2006

The most shielded CS and smallest QC component are nearly normal to the peptide plane, and the largest QC component lies in the peptide plane perpendicular to the C═O bond. The in-plane CS components are rotated relative to the molecular axes such that the most deshielded (downfield) component is 17° off of the C═O bond. This is very close to the calculated molecular orientations reported for benzamide, benzanilide, *N*-methylbenazamide, and acetanilide.[8,10] The central residue tensor span in the more strongly H-bonded GGV ($\delta_{span} = 549 \pm 8$ ppm) is significantly smaller than in AGG ($\delta_{span} = 606 \pm 8$ ppm), indicating the effects of intermolecular interactions, which are modeled by DFT calculations of isolated molecules and trimers. The latter contain direct and indirect H-bonded neighbors in the crystal lattice and predict principal axis orientations within 7° of experiment and CS principal components with an rmsd of 16 ppm. Comparison with the monomer calculations indicates that the smaller ^{17}O shielding span in GGV is primarily a consequence of two factors: (i) a stronger direct H bond at the target oxygen and (ii) indirect H bonding at the NH group to a carboxylate ion.

Experimental Methods

Peptide Synthesis ^{17}O was incorporated into Boc-Gly via basic exchange with $H_2{}^{17}OH$. Boc-Gly (0.171 mmol) was added to a $Na^{17}OH$ solution that was prepared by adding approximately 1 mg of Na(s) to 20 μL of 40% $H_2{}^{17}O$ (0.444 mmol ^{17}O) in a sealed 4 mm glass tube and held at 47 °C for 72 h. Boc-[^{17}O]-Gly was extracted iteratively at 0° C with ethyl acetate after acidification to pH 2 by addition of 6 M HCl. Isotopic labeling was estimated to be 34% using electrospray mass spectrometry. Since ^{17}O labels are distributed between both carboxylic acid oxygen sites, effective labeling at the carbonyl oxygen was 17%. Ala-[^{17}O]Gly-Gly (A*GG) and Gly-[^{17}O]Gly-Val (G*GV) were prepared by standard *t*-Boc solid-phase synthesis.[14] The extent of coupling was monitored by microscopic observation of peptide resin beads treated with 5% ninhydrin/ethanol. Coupling was deemed complete when all traces of purple were absent. A 1.1-fold molar excess of Boc-[^{17}O]Gly was coupled to the resins using equimolar amounts of 1-hydroxybenzotriazole (HOBT) and Castro's reagent (BOP) in DMF for 3 h. The N-terminal residues of A*GG and G*GV were coupled by adding 6-fold molar excesses of unlabeled Boc-Ala and Boc-Gly, respectively, along with HOBT, and 1,3-dicyclohexylcarbodiimide (DCC). Peptides were cleaved from the resin with anhydrous HF[14] and extracted with 25% acetic acid. Following lyophyllization, peptides suitable for single-crystal growth were obtained by purifying crude peptides with cation-exchange chromatography (Dowex 50X8-100).

NMR Spectroscopy. ^{17}O NMR single-crystal spectra were acquired at 11.7 T (^{17}O frequency of 67.15 MHz) on a home-built spectrometer with a double-resonance (^1H, ^{17}O) goniometer probe based on a previously described design.[15] ^{17}O single-crystal spectra were acquired with 3−5 s recycle delays using two-level Hartman−Hahn contacts[16] followed by ^1H decoupling (50 kHz). Experimental line widths were 2−5 ppm, and spectra with S/N ≥ 15 were accumulated in less than 1000 transients, Figure 1, with crystals weighing 1−3 mg. Orientation-dependent NMR frequencies were sampled in 7° increments over a range ≥200° for three orthogonal axes.

Static powder spectra were excited by cross-polarization, and echoes were acquired with ^1H CW decoupling. MAS powder spectra, 14.1 T, were acquired with a Hahn echo and CW decoupling. Frequencies were referenced externally to $H_2{}^{17}O$-(l).

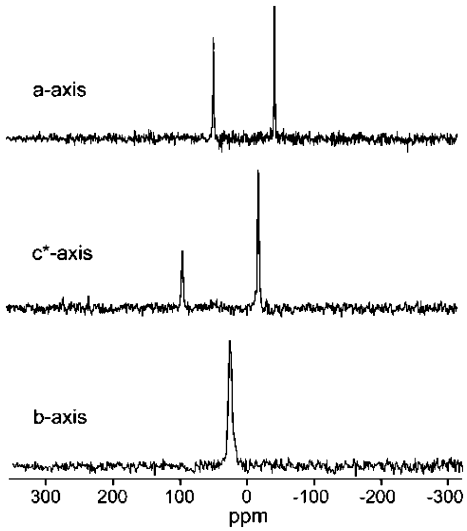

Figure 1. ^{17}O spectra (∼1k transients) from a 1 mg GGV crystal. On the basis of the enrichment level (17%), the spectra correspond to detection of ∼0.4 μm.

Crystal Growth and Mounting. G*GV and A*GG crystals weighing 0.9−3 mg with clearly defined faces were grown by vapor diffusion against ethylene glycol inside silanized glass chambers. X-ray crystallography was used to confirm crystal space groups and determine unit cell orientations with respect to morphological faces. Crystallographic symmetry was exploited to independently confirm the location of unit cell axes in the NMR experiments. Since both GGV·$2H_2O$ (CSD = CUWRUH)[17] and AGG·H_2O (CSD = CALXES20)[18] crystallize in a monoclinic space group, $P2_1$, two NMR lines are expected for the general orientation and a single line if the crystal is rotated about the *b* axis. Hence, the two molecules in the unit cell are chemically equivalent but magnetically inequivalent for a general orientation in the magnetic field. This feature was used to identify the *b* axis, where the two molecules of the unit cell give identical projections onto the static magnetic field, and to fine adjust crystal mounting. Additional structural details, including the atomic coordinates, can be obtained at www.ccdc.cam.ac.uk/conts/retrieving.html.

Single-Crystal Data Analysis. Observed central transition frequencies were modeled as the sum of first-order chemical shielding, ν_{CS}, and second-order quadrupole coupling, ν_{QC}.[13,16] In a frame with the *Z* axis along $\mathbf{B}_0$ and the *Y* axis parallel to the goniometer axis, the chemical shielding and quadrupole coupling contributions are given by

$$\nu_{CS} = -\sigma_{zz}\nu_0 \tag{1}$$

and

$$\nu_{QC} = \frac{1}{1600\nu_0}[8(\chi_{XX} - \chi_{YY})^2 + 32\chi_{XY}{}^2 - 64(\chi_{XZ}{}^2 + \chi_{YZ}{}^2)] \tag{2}$$

where ν_0 is the Larmor frequency and $\chi_{ij} = e^2Qq_{ij}/h$. Rotations through ϕ about *Y* tranform ν_{CS} and ν_{QC} according to $R_Y{}^T(\phi)\sigma R_Y(\phi)$ and $R_Y{}^T(\phi)\chi R_Y(\phi)$. Consequently, the observed frequency has the following form

$$\nu_{obs}{}^Y(\phi) = C_1{}^Y + C_2{}^Y\cos(2\phi) + C_3{}^Y\sin(2\phi) + C_4{}^Y\cos(4\phi) + C_5{}^Y\sin(4\phi) \tag{3}$$

Expressions relating $C_i{}^Y$ to CS and QC tensor components have

been given previously,[13] and C_i^Y were determined experimentally by least-squares fitting eq 3 to the NMR rotation data. Cyclic permutation of the coordinates, $X = a$, $Y = b$, and $Z = c^*$, gives 15 equations from which the 11 independent elements of the CS and QC tensors were determined. Pairs of tensors related by crystallographic symmetry were extracted by first solving all possible subsets of the six nonlinear algebraic equations involving C_4^i and C_5^i for the traceless, symmetric QC tensor using a Levenburg−Marquardt algorithm. By randomly varying the initial parameter estimates, multiple solutions were found and those with quadrupole couplings outside the expected range ($6.5 < |\chi| < 9.5$ MHz) were discarded. For both GGV and AGG, two tensors with different eigenvalues satisfied this criterion and were used as input into the remaining nine equations. Solving these equations results in double determination of the CS components, and averages of the two values were used to construct all possible shielding tensors consistent with experiment. To each of the QC tensors, two CS tensors with distinct eigenvalues were found. Spurious solutions result from (i) the nonlinear dependence on the QC components and (ii) using rotation axes that coincide with crystal symmetry axes. The correct CS and QC tensors were selected by comparison of experimental powder patterns with calculated patterns based on all tensor combinations consistent with the single-crystal data. Static powder patterns obtained at 21.2 T were particularly useful since they displayed five well-resolved peaks or shoulders.

The possibility of obtaining accurate CS and QC parameters from the 21.2 T powder spectra alone was examined by a Monte Carlo search in which the eight parameters describing the spectrum (CS and QC principal components and the three Euler angles specifying their relative orientation) were treated as random numbers within a specified range of initial parameters guesses. The eight parameters, set by a random number generator, were used to calculate a powder pattern that was compared with experiment and either retained or, if any of the five peaks or shoulders differed from experiment by more than 10 ppm, discarded. After n repetitions, histograms of the retained parameters were found to be tightly grouped about their average values. Consequently, averages and standard deviations of these distributions were taken as the "best-fit" parameter values and uncertainty limits for comparison with parameters determined in the single-crystal experiments. DFT calculations, for example, provided adequate parameter guesses, and $n \approx 10^6$ Monte Carlo steps were sufficient to explore the space encompassed by ±0.5 MHz in χ, ±0.21 in η, ± 25 ppm in CS components, ±25° in α, ±3° in β, and ±10° in γ.

Theoretical Calculations. ^{17}O shielding tensors were calculated with density functional theory (DFT) and the gauge including atomic orbitals (GIAO)[19−22] approach as implemented in Gaussian 98.[23] Trimer clusters of GGV and AGG were constructed from CSD coordinates and include the effects of indirect and direct hydrogen bonding. Hydrogen coordinates were optimized at B3LYP/6-31g(d). B3LYP functionals were used with aug-cc-pvdz and 6-311++g(d, p) basis sets for NMR calculations. Electric field gradient components were related to quadrupole tensor components, χ_{ij}, by $\chi_{ij} = e^2q_{ij}Q/h = -2.3496Qq_{ij}$.[8] Using the accepted value of Q (−2.558),[24] $\chi_{ij} = 6.01q_{ij}$ MHz. DFT CS components were converted into chemical shifts, δ_{ii}, relative to liquid H_2O by subtracting calculated shifts from 307.9 ppm.[24]

Results and Discussion

CS and QC Tensor Determinations. Representative single-crystal spectra are shown in Figure 1, and the graphs of NMR frequency versus rotation angle are presented in Figure 2. Observation of single lines in the b-axis rotations and curve crossings at 0° and 90° for symmetry-related pairs in the a and c^* rotations, Figure 2, are fully consistent with the space group symmetry $P2_1$. These data do not, however, uniquely determine the tensors since several combinations of possible CS and QC tensors are consistent with the data (see Experimental Section). To identify the correct solution, all possible single-crystal solutions were used to simulate static or MAS powder spectra at three field strengths, 11.7, 21.2, and 14.1 T, and these were compared to experiment. Only the single-crystal solutions listed in Tables 1 and 2 and superimposed on the powder spectra in Figure 3 are consistent with the prominent features of the experimental spectra. Moreover, the 21.2 T powder patterns, which show five well-resolved features, were independently "fit" by a Monte Carlo search (see Experimental Section). Although

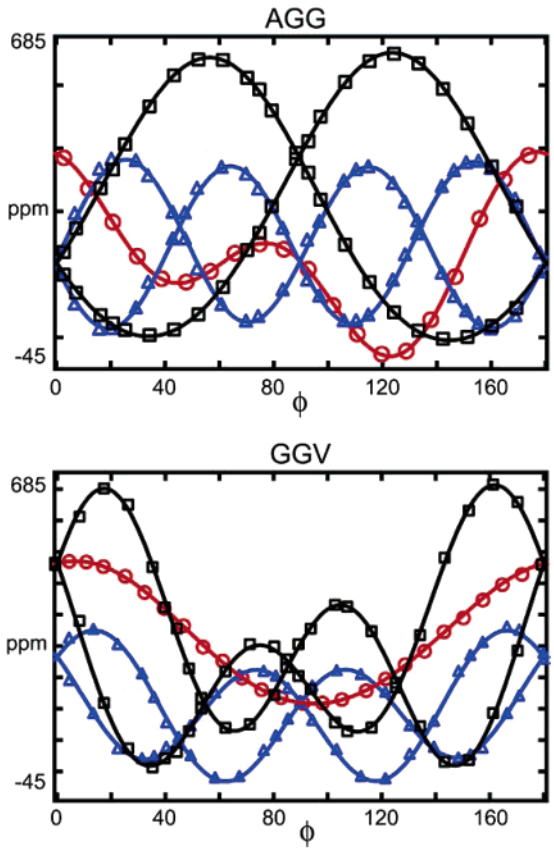

Figure 2. ^{17}O NMR frequencies as a function of crystal orientation for A*GG and G*GV. Frequencies for symmetry-related pairs are shown for crystal rotations about the a (squares), b (circles), and c^* (triangles) axes.

TABLE 1: G*GV and A*GG QC Tensors[a]

	χ_{xx}	χ_{yy}	χ_{zz}	x	y	z
GGV	−3.04(0.019)	−5.52(0.05)	8.56(0.05)	plane	orthog	C═O
a	0.178	−0.946	0.272	0.270	0.236	−0.933
b	0.194	0.305	0.933	0.941	0.142	0.308
c^*	0.965	0.113	−0.237	−0.205	0.961	0.184
AGG	−3.37(0.17)	−5.19(0.19)	8.57(0.14)	plane	orthog	C═O
a	0.416	−0.201	−0.887	−0.891	0.329	−0.313
b	0.591	−0.682	0.431	0.454	0.609	−0.650
c^*	0.692	0.703	0.165	0.023	0.721	0.692

[a] The principal components (MHz) are in bold, and the corresponding eigenvectors and reference vectors are in the crystal (a, b, c^*) frame. Reference vectors x and y are in the peptide plane and orthogonal to the peptide plane, respectively, and z is collinear with the carbonyl bond.

TABLE 2: G*GV and A*GG CS Tensors[a]

	δ_{11}	δ_{22}	δ_{33}	*x*	*y*	*z*
GGV	526(5)	388(5)	−23(3)	plane	orthog	C═O
a	−0.819	0.540	0.192	0.270	0.236	−0.933
b	0.570	0.803	0.172	0.941	0.142	0.308
*c**	0.061	−0.250	0.966	−0.205	0.961	0.184
AGG	546(6)	405(6)	−60(6)	plane	orthog	C═O
a	−0.432	−0.804	0.407	−0.891	0.329	−0.313
b	−0.516	0.591	0.620	0.454	0.609	−0.650
*c**	0.740	−0.058	0.671	0.023	0.721	0.692

[a] Principal components (ppm) are in bold, and the corresponding eigenvectors and reference vectors are in the crystal (*a*, *b*, *c**) frame. Reference vectors are identical to those in Table 1.

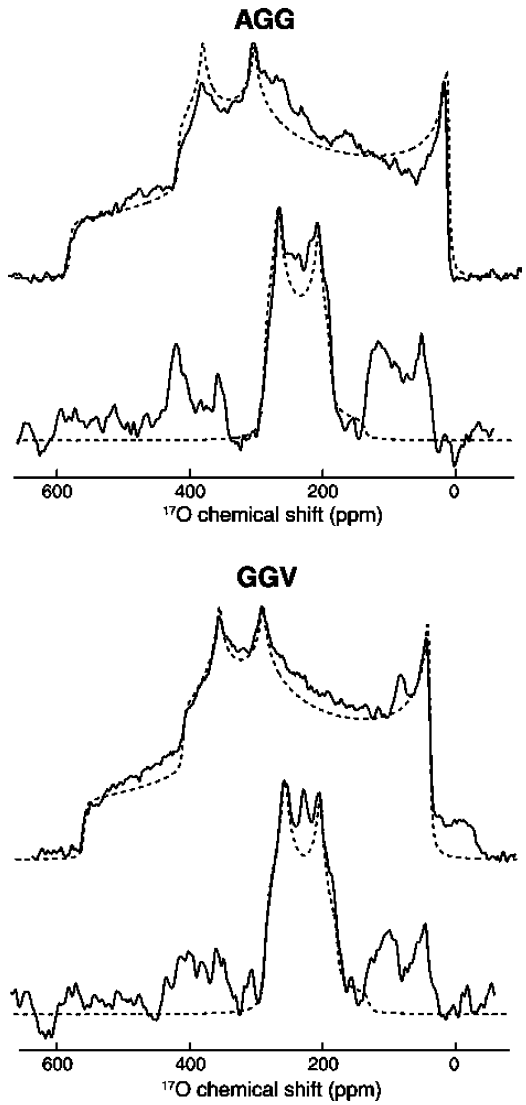

Figure 3. Static 21.2 T (top) and MAS (14.1 T) experimental (solid) and simulated (dashed) powder patterns for A*GG and G*GV. The simulation parameters are the QC and CS tensor components determined from the single-crystal experiment, Tables 1 and 2, that correctly predict the powder patterns.

the fitting procedure might appear to be under determined, given reasonable initial guesses the eight parameters determined are unique within the stated uncertainty limits and in excellent agreement with the crystal values, Table 3. Finally, experimental tensor orientations are also in reasonable agreement with the DFT calculations presented below, and these were used to make the complete assignment of symmetry-related tensors to individual molecules in the unit cell. The existence of a unique solution based on a combination of experimental techniques provides compelling evidence that the correct single-crystal solution was determined. The CS and QC principal components and molecular orientations are summarized for the two peptides in Figure 4.

Overall, the QC principal components are within 8° of the molecular axes, Table 1 and Figure 4. The smallest component is normal to the peptide plane, and the largest component is in the peptide plane and perpendicular to the C═O bond. In both peptides, the most shielded CS component is normal to the peptide plane while the in-plane components are rotated 17° toward C^{α} with the most deshielded component, δ_{11}, closest to the C═O bond. Although isotropic shifts are the same in the two peptides, the GGV tensor span, δ_{span}, is significantly smaller. Compared to AGG, δ_{11} and δ_{22} are downfield by 20 and 27 ppm, respectively, and δ_{33} is upfield by 34 ppm.

Effects of structure and intermolecular interactions on the CS and QC tensor parameters are conveniently modeled by quantum chemical calculations wherein structural features such as H-bonding distances and conformations can be systematically added or otherwise altered. For example, model calculations in a methylacetamide:formamide dimer[8] showed that as *r*(O···N) increases, δ_{11} and δ_{22} move downfield and δ_{33} moves upfield. With *r*(O···N) distances of 2.777 (GGV) and 2.926 Å (AGG), the NMR data, Table 2, is consistent with this trend. Experience with ^{15}N DFT calculations also suggests that indirect H bonding to the peptide NH groups could also effect ^{17}O shielding. To address these possibilities, we compare experiment with DFT calculations, Table 4, of monomeric species and trimer clusters of AGG and GGV constructed from their respective X-ray coordinates. The monomers are zwitterionic species without H bonding, and the trimeric clusters, $(GGV)_3$ and $(AGG)_3$, include indirect and direct H bonding and charge neutralization[11] at the termini as a result of salt bridges in the X-ray structure, Figure 5. We note that the clusters are small in the sense that they contain the minimum number of formula units required to incorporate the complete H-bonding patterns observed in the X-ray structures. Locally dense DFT calculations using two basis sets, 6-311++g(d,p) and aug-cc-pvdz, are compared with experiment in Table 4. Previously, aug-cc-pvdz was used to accurately predict both the gas-phase QC coupling in water (χ = 10.18 MHz) and the much smaller ice coupling (χ = 6.66 MHz) which was modeled as a 42-molecule cluster.[13] In the present case, the aug-cc-pvdz trimer calculations more accurately predict QC and CS parameters (rmsd = 16 ppm) than the 6-311++g(d,p) trimers (rmsd = 44 ppm). Thus, only results based on the larger aug-cc-pvdz basis set are discussed further. We note that correlating the two sets of calculations shows a precise linear relation, $\delta^{aug.} = 0.935\delta^{6-311} - 10$, that could be used to scale the less computationally intensive 6-311++g(d,p) CS parameters for improved accuracy. Scaling of the aug-cc-pvdz trimer calculations does not significantly improve agreement with experiment. Similar calculations were previously reported for dimers of small neutral amides ([^{17}O]benzanilide, [^{17}O]*N*-methyl-benzamide, and [^{17}O]acetanilide); rmsd errors of calculated versus experimental CS parameters were 54−55 ppm compared to 15−17 ppm for trimer calculations reported here. Improved agreement with experiment for tripeptides studied here versus the previously reported amides results in part from the use of larger clusters. Although agreement could potentially be improved by further increasing cluster size, this was not pursued since the goal here is to understand the extent to which experiment can be interpreted in terms of local interactions. With this in mind, we conclude that with the computational methods

TABLE 3: Comparison of Peptide ^{17}O CS and QC Parameters Determined by 11.7 T Single-Crystal (xtal) and 21.2 T Powder NMR Experiments[a]

peptide	χ_{zz}	η	δ_{11}	δ_{22}	δ_{33}	(α, β, γ)
G*GV (xtal)	8.56(0.08)	0.29(0.02)	526(5)	388(5)	−23(3)	−1(3), 91(3), 73(3)
G*GV (powder)	8.54(0.28)	0.32(0.13)	528(8)	396(6)	−33(8)	0(2), 91(1), 74(2)
A*GG (xtal)	8.57(0.14)	0.21(0.03)	546(6)	405(6)	−60(6)	−2(3), 89(3), 74(3)
A*GG (powder)	8.55(0.29)	0.19(0.13)	543(9)	403(6)	−55(8)	5(3), 89(1), 73(2)

[a] The quadrupolar coupling, χ, is in MHz, δ_{ii} are in ppm, and (α, β, γ) are the Euler angles (deg) describing the transformation from the CS to the QC principal axis frames.

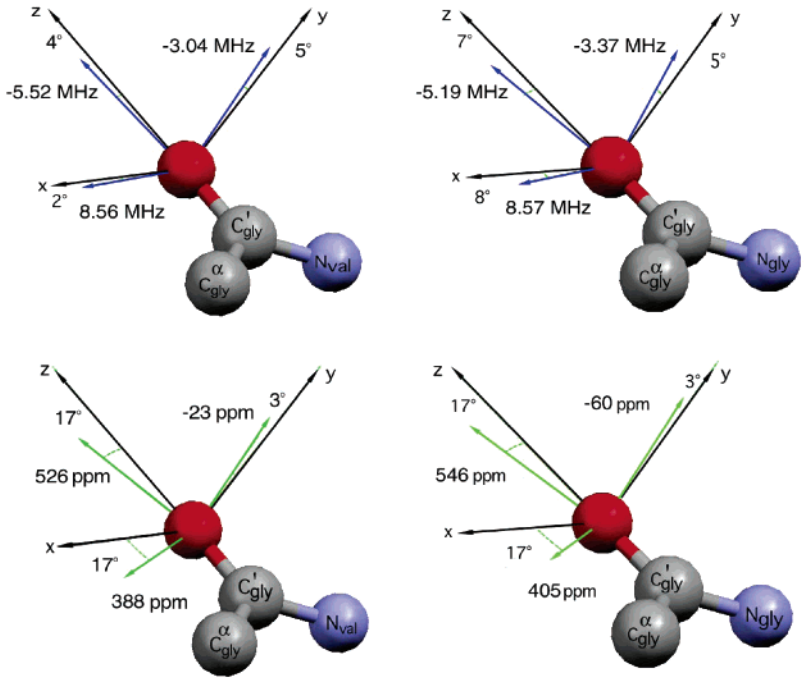

Figure 4. Principal QC and CS axes in the molecular frame of G*GV (left) and A*GG (right). Reference vectors *x* and *y* are in the peptide plane and orthogonal to the peptide plane, respectively, and *z* is collinear with the carbonyl bond.

TABLE 4: DFT and Experimental ^{17}O CS and QC Tensors[a]

G*GV	χ	η	δ_{11}	δ_{22}	δ_{33}	δ_{span}	δ_{dev}	δ_{iso}	(δ_{11}&z, δ_{22}&x, δ_{33}&y)	(χ_{xx}&y, χ_{yy}&z, χ_{zz}&x)
mon, a	9.25	0.27	657	475	−20	677	495	371	(13°, 13°, 2°)	(19°, 19°, 2°)
mon, b	9.87	0.24	715	521	−11	726	532	408	(14°, 14°, 2°)	(22°, 22°, 2°)
tri, a	8.85	0.38	547	408	−19	566	427	312	(16°, 15°, 3°)	(6°, 6°, 0°)
tri, b	9.41	0.36	592	447	−9	601	456	343	(16°, 16°, 3°)	(6°, 6°, 0°)
exp.	8.56	0.29	526	388	−23	549	411	297	(17°, 17°, 3°)	(2°, 4°, 5°)
A*GG										
mon, a	8.46	0.24	578	395	−52	630	447	307	(15°, 15°, 1°)	(3°, 3°, 0°)
mon, b	9.01	0.20	627	436	−45	672	481	339	(15°, 15°, 1°)	(3°, 3°, 0°)
tri, a	8.62	0.29	550	389	−40	590	429	300	(13°, 13°, 1°)	(1°, 1°, 1°)
tri, b	9.17	0.25	593	430	−34	628	464	330	(13°, 13°, 1°)	(1°, 1°, 1°)
exp.	8.57	0.21	546	405	−60	606	465	297	(17°, 17°, 3°)	(8°, 7°, 5°)

[a] DFT calculations are for monomeric (mon) and trimeric (tri) clusters using the aug-cc-pvdz (a) and 6-311++g(d,p) (b) basis sets. The quadrupolar coupling, χ (MHz), CS components (ppm), and angles (deg) for the CS or QC principal components in the local molecular frame are as defined in Tables 1 and 2 and shown in Figure 4. Reference vectors *x* and *y* are in the peptide plane and orthogonal to the peptide plane, respectively, and *z* is collinear with the carbonyl bond.

used here, theoretical error bounds for the calculations presented are ∼20 ppm. For example, the relative sizes of the $(GGV)_3$ and $(AGG)_3$ tensor spans are correctly predicted, but the $(GGV)_3$ calculation overestimates the span by 17 ppm, and the $(AGG)_3$ calculation underestimates the span by 16 ppm.

DFT calculations[8] of several neutral organic molecules indicate a systematic effect of H bonding on shielding. H bonding with r(O···N) = 2.93 Å decreases the tensor span by ∼80 ppm with a distance dependence of −90 ppm/Å. In the two cases studied here, r(O···N) = 2.777 Å (GGV) and r(O···N) = 2.926 Å (AGG), span decreases of ∼90 ppm for GGV or ∼80 ppm for AGG are indicated, i.e., values that are only in fair agreement with those calculated from Table 4, −111 ppm for GGV or −40 ppm for AGG. An important distinction is that the peptides studied here are not neutral. In this regard, there are two structural differences between GGV and AGG that would affect the electric field in the neighborhood of the target peptide group. First, the helix-like GGV structure places the terminal carboxylate much closer to the target carbonyl than in the extended AGG structure. Second, and likely more

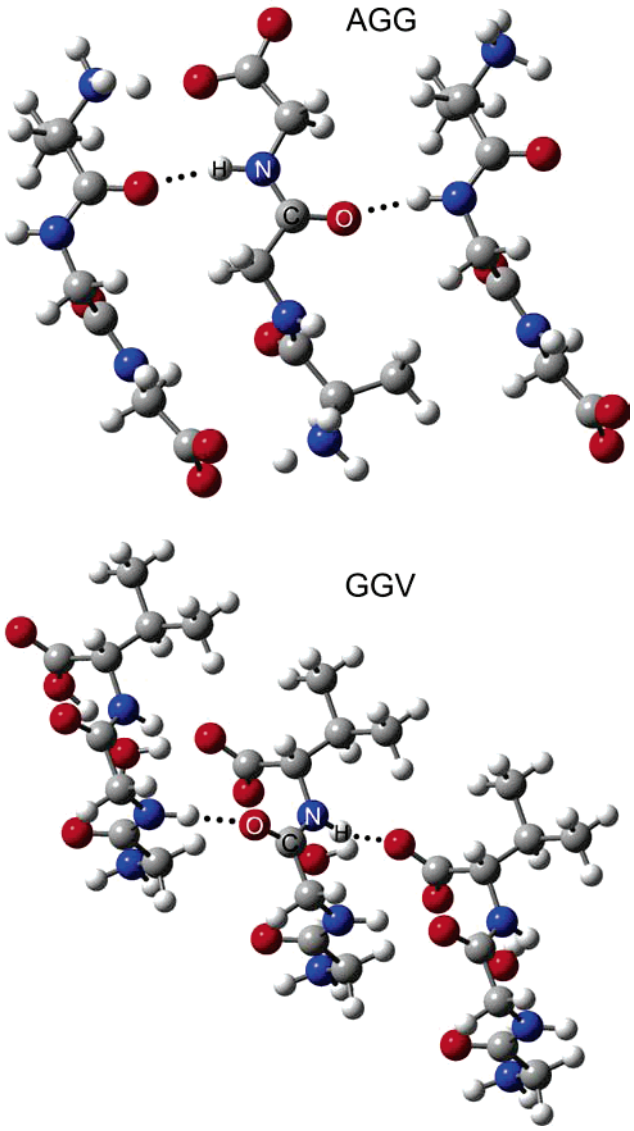

Figure 5. Trimers of AGG and GGV. The central carbonyl amide group of each tripeptide interacts with neighboring tripeptide molecules through hydrogen bonding. The central amide N−H interacts by intermolecular hydrogen bonding with a neighboring O═C in AGG, with $-COO^-$ in GGV. Atom color codes are as follows: red, oxygen; blue, nitrogen; gray, carbon; white, hydrogen.

important for reasons of proximity, the indirect H bond in GGV is to a carboxylate while in AGG it is to a carbonyl. Although the limited set of calculations presented here do not allow us to parse the observed shielding parameters into individual effects, we conclude that nearby charged groups have a substantial impact, $\geq$20 ppm, on ^{17}O shielding.

Conclusions

The primary results reported here are the first experimental determination of ^{17}O CS and QC tensors in peptides. Differences in central residue peptide oxygen CS principal components between the two peptides are in the range of 15−30 ppm and correlate with differences in the strength of the direct H bond and the charge on the indirect H-bond partner. By contrast, QC and CS principal axes are the same in the two peptides. The QC principal axes are coincident with local molecular axes, the peptide plane normal and the C═O bond. The in-plane CS axes are rotated such that the most deshielded component is 17° away from the C═O bond and closer to C^α, Figure 4. These tensor orientations are in excellent agreement with orientations reported for non-peptide amides that were arrived at using a combination of powder NMR experiments and DFT calculations.[8]

The NMR parameters most sensitive to structure are the CS and QC principal components. Thus, reliable powder sample experiments for obtaining these are inherently more general and less arduous since single crystals and a large number of spectra are not required. In the two cases examined here, a brute-force Monte Carlo search applied to the 21.2 T powder spectra found unique sets of QC and CS parameters that are in excellent agreement with the single-crystal results. The approach makes use of initial parameter guesses and depends only on well-defined spectral features,[25] so it is independent of the intensity distortions typically encountered in these experiments. In practice, a very high field instrument (21.2 T) is essential since the relevant spectral features are far better resolved as a result of reducing the inhomogeneous second-order QC broadening. Consequently, CS principal components are more accurately determined than QC components.

DFT calculations demonstrate that detailed information about intermolecular interactions is available from the O^{17} NMR parameters. Calculated tensors from nominal clusters that incorporate the H-bond interactions seen in the X-ray structures are in far better agreement with experiment than those from isolated molecules. Thus, DFT parameters can provide a means for interpreting NMR data as well as initial guesses for extracting NMR parameters from powder experiments. Two basis sets were examined in this study, and CS principal components from the larger, correlation-consistent aug-cc-pvdz set are in significantly better agreement with experiment. Frequently, DFT NMR parameters are empirically scaled to account for basis set truncation and/or neglect of lattice interactions. Although scaling the aug-cc-pvdz cluster calculations by correlating with experiment does not significantly improve agreement, scaling parameters from the smaller basis set, 6-311++g(d,p), by correlating with the larger set significantly improves agreement of the CS but not the QC parameters.

We anticipate that the results presented here should stimulate further interest in structural studies of proteins by solid-state ^{17}O NMR. The methods used here have been recently applied to biologically interesting polypeptides,[26,27] and we have shown that the ^{17}O NMR experiment monitors key features including local electrostatics and H bonding.[28] The results presented here, which unambiguously determine the molecular orientations of the QS and CS tensors and the characteristic magnitudes of the corresponding principal components, are essential in several contexts. They provide stringent tests of quantum chemical methods, are essential guides for structural analysis of spectra from oriented sample spectra, and drastically reduce the parameter space that needs to be searched to determine CS and QC principal components from spectra of unoriented samples.

Acknowledgment. We thank Professor Tim Cross for financial support (E.Y.C., NSF MCB-0235774) and providing access to the 21.2 T instrument at the NHFML supported by NSF Cooperative agreement (DMR 00884173) and the State of Florida, Dr. Mark Mashuta and Dr. Sean Parkin for indexing the crystals, Dr. William Pierce and Ned Smith for determining isotope labeling by mass spectrometry, and the University of Kentucky super computer center for access to the HP Superdome computing facility.

References and Notes

(1) Mueller, K. T.; Sun, B. Q.; Chingas, G. C.; Zwanziger, J. W.; Terao, T.; Pines, A. *J. Magn. Reson.* **1990**, *86*, 470−487.

(2) Llor, A.; Virlet, J. *Chem. Phys. Lett.* **1988**, *152*, 248−253.
(3) Chmelka, B. F.; Mueller, K. T.; Pines, A.; Stebbins, J.; Wu, Y.; Zwanziger, J. W. *Nature* **1989**, *339*, 42−43.
(4) Samoson, A.; Lippmaa, E.; Pines, A. *Mol. Phys.* **1988**, *65*, 1013−1018.
(5) Wu, Y.; Sun, B. Q.; Pines, A.; Samoson, A.; Lippmaa, E. *J. Magn. Reson.* **1990**, *89*, 297−309.
(6) Frydman, L.; Harwood, J. S. *J. Am. Chem. Soc.* **1995**, *117*, 5367−5368.
(7) Pike, K. J.; Lemaitre, V.; Kukol, A.; Anupold, T.; Samoson, A.; Howes, A. P.; Watts, A.; Smith, M. E.; Dupree, R. *J. Phys. Chem. B* **2004**, *108*, 9256−9263.
(8) Yamada, K.; Dong, S.; Wu, G. *J. Am. Chem. Soc.* **2000**, *122*, 11602−11609.
(9) Chekmenev, E. Y.; Zhang, Q.; Waddell, K. W.; Mashuta, M. S.; Wittebort, R. J. *J. Am. Chem. Soc.* **2004**, *126*, 379−384.
(10) Wu, G.; Yamada, K.; Dong, S.; Grondey, H. *J. Am. Chem. Soc.* **2000**, *122*, 4215−4216.
(11) Waddell, K. W.; Chekmenev, E. Y.; Wittebort, R. J. *J. Am. Chem. Soc.* **2005**, *127*, 9030−9035.
(12) Chekmenev, E. Y.; Xu, R. Z.; Mashuta, M. S.; Wittebort, R. J. *J. Am. Chem. Soc.* **2002**, *124*, 11894−11899.
(13) Zhang, Q.; Chekmenev, E. Y.; Wittebort, R. J. *J. Am. Chem. Soc.* **2003**, *125*, 9140−9146.
(14) Stewart, J. M.; Young, J. D. *Solid-Phase Peptide Synthesis*, 2nd ed.; Pierce Chemical Co.: Rockford, 1984.
(15) Zhang, Q. W.; Zhang, H.; Lakshmi, K. V.; Lee, D. K.; Bradley, C. H.; Wittebort, R. J. *J. Magn. Reson.* **1998**, *132*, 167−171.
(16) Zhang, Q. W.; Zhang, H. M.; Usha, M. G.; Wittebort, R. J. *Solid State Nucl. Magn. Reson.* **1996**, *7*, 147−154.
(17) Lalitha, V.; Subramanian, E.; Bordner, J. *Int. J. Pept. Protein Res.* **1984**, *24*, 437−441.
(18) Subramanian, E.; Lalitha, V. *Biopolymers* **1983**, *22*, 833−838.
(19) Ditchfield, R. *Mol. Phys.* **1974**, *27*, 789−807.
(20) London, F. *Phys. Radium* **1937**, *8*, 397.
(21) Rauhut, G.; Puyear, S.; Wolinski, K.; Pulay, P. *J. Phys. Chem.* **1996**, *100*, 6310−6316.
(22) Wolinski, K.; Hinton, J. F.; Pulay, P. *J. Am. Chem. Soc.* **1990**, *112*, 8251−8260.
(23) Frisch, M. J.; et al. *Gaussian 98*, Revision A.7; Gaussian, Inc.: Pittsburgh, PA, 1998.
(24) Wasylishen, R. E.; Mooibroek, S.; Macdonald, J. B. *J. Chem. Phys.* **1984**, *81*, 1057−1059.
(25) Oas, T. G.; Drobny, G. P.; Dahlquist, F. W. *J. Magn. Reson.* **1988**, *78*, 408−424.
(26) Chekmenev, E. Y.; Waddell, K. W.; Hu, J.; Gan, Z.; Wittebort, R. J.; Cross, T. A. *J. Am. Chem. Soc.* **2006**, *128*, 9849−9855.
(27) Fu, R., et al. *J. Magn. Reson.* **2005**, *177*, 1−8.
(28) Hu, J.; Chekmenev, E. Y.; Gan, Z. H.; Gor'kov, P. L.; Saha, S.; Brey, W. W.; Cross, T. A. *J. Am. Chem.* Soc. **2005**, *127*, 11922−11923.